Textures and Microstructures, 1988, Vol. 7, pp. 265–301
Reprints available directly from the publisher
Photocopying permitted by license only

Printed in the United Kingdom

Role of Twinning in Texture Development and in Plastic Deformation of Hexagonal Materials

M. J. PHILIPPE,† C. ESLING† and B. HOCHEID‡

† *Laboratoire de Métallurgie des Materiaux Polycristallins, UER Sciences, F-57045 Metz Cedex 01*
‡ *Laboratoire de Métallurgie CNAM, 292 rue St Martin, F-75141 Paris Cedex*

(Received June 20, 1987; in final form December 4, 1987)

This paper presents an extensive study of the conditions of appearance of mechanical twinning and its role in the texture development during uniaxial tension, biaxial expansion and rolling of Ti and Zr alloys.

With the help of literature, the analyses are extended to alloys of Mg, Zn and Be.

Finally, the influence of twinning on the shape of the forming limit diagrams and on formability is discussed for hexagonal metals.

KEY WORDS: Titanium, Zirconium, Mechanical twinning, Texture development, Tension, Rolling, Biaxial expansion, Forming limit diagrams.

INTRODUCTION

The modelization of the polycrystalline plasticity according to the well-known theories of Bishop-Hill (1951) and Taylor (1938), currently requires grains having 5 independent deformation mechanisms in order to accommodate any imposed strain. If most metals of cubic structure possess five and more independent glide systems, this is not the case for hexagonal metals. For the latter metals, the

most common basal and prismatic glide modes have only 2 or 3 independent glide systems respectively (Groves, 1963). Secondary systems like pyramidal glide with $c + a$ Burgers vector can then contribute to the deformation, but in many cases twinning becomes active, (Yoo, 1981 and Partridge, 1967).

The role of twinning is not always clear because it is difficult to isolate this mechanism and thus to deduce its effects on the ductility, which gives rise to controversy (Keshavan *et al.*, 1975; Reed-Hill, 1972 and Reed-Hill *et al.*, 1975). This study on Ti and Zr alloys aims at detailing

—the appearance of twinning
—its effect on the evolution of texture during uniaxial tension, biaxial expansion and rolling
—its influence on the forming limit diagrams and the formability.

The materials used

For our investigation we used Ti and Zr sheets kindly provided by the company CEZUS. The initial material had a thickness of 1 mm and had already been deformed at about 50% by cold rolling. The chemical analyses of the ingots out of which the sheets had been manufactured are given in Table 1, where QN stands for Qualité Nucléaire, i.e. nuclear grade.

Starting from pure Ti and Zr, we made additional alloys whose compositions are given in Table 2. The manufacturing schedule was identical to that of the above mentioned sheets. All sheets were annealed for 1 hr at 650°C.

Table 1 Chemical composition of the common grades T 35 and Zr QN.

In ppm in weight	C	O	N	Fe	Si	H
Titanium (T 35)	150	900	80	400	100	30
Zirconium (Zr QN)	75	1000	40	380	50	5

Table 2a Various Ti-alloys prepared starting from pure Ti. The usual commercial denomination T 35 corresponds to the grade $T9O_24Fe$

		Rates in ppm of weight			
	Denomination	O_2	Fe	N_2	Grain size
	$T5O_2$	500			~50 μ
	$T8O_2$	800			~50 μ
	$T5O_2$ 3Fe	500	350		~50 μ
	$T9O_2$ $4Fe_{T35}$	900	400	80	~40 μ
Titanium	$T18O_2$ 4Fe	1800	400	80	~40 μ
	$T25O_2$ 4Fe	2500	400	80	~40 μ
	$T9O_2$ 7Fe	900	700	80	~30 μ
	$T9O_2$ 10Fe	900	1000	80	~20 μ
	$T9O_2$ 4Fe $1N_2$	900	400	150	~40 μ
	$T9O_2$ 4Fe $3N_2$	900	400	300	~40 μ

Table 2b Various Zr-alloys prepared starting from pure Zr. The usual commercial denomination ZrQN corresponds to the grade $Z9O_23Fe$.

		Rates in ppm of weight			
	Denomination	O_2	Fe	N_2	Grain size
	$Z3O_2$	350			~40 μ
	$Z8O_2$	800			~40 μ
	$Z5O_2$ 3Fe	500	340		~40 μ
	$Z9O_2$ $3Fe_{ZrQN}$	900	340	24	~30 μ
	$Z18O_2$ 3Fe	1800	340	24	~30 μ
Zirconium	$Z25O_2$ 3Fe	2500	340	24	~30 μ
	$Z9O_2$ 7Fe	900	700	24	~20 μ
	$Z9O_2$ 10Fe	900	1000	24	~15 μ
	$Z9O_2$ 3Fe $1N_2$	900	340	150	~30 μ
	$Z9O_2$ 3Fe $3N_2$	900	340	300	~30 μ

Rolling texture and texture development by tension or biaxial expansion

The textures of the various Ti specimens are similar except for those with high O_2-content (Figure 1). The {0002}-pole figures (PFs) show two strong maxima at ±35° inclined from ND towards TD. The $\{10\bar{1}0\}$-PFs display a preferred orientation parallel to RD. The {0002}-PFs of the samples with higher O_2-content ($T25O_24Fe$–2500 ppm O_2) show a smaller tilt angle out of ND, and additional—but weak—maxima inclined towards RD. The PFs of Zr with low O_2 content are very similar to those of Ti, except for a tilt of the *c*-axes of about 25°. The other sheets with a higher O_2-content have

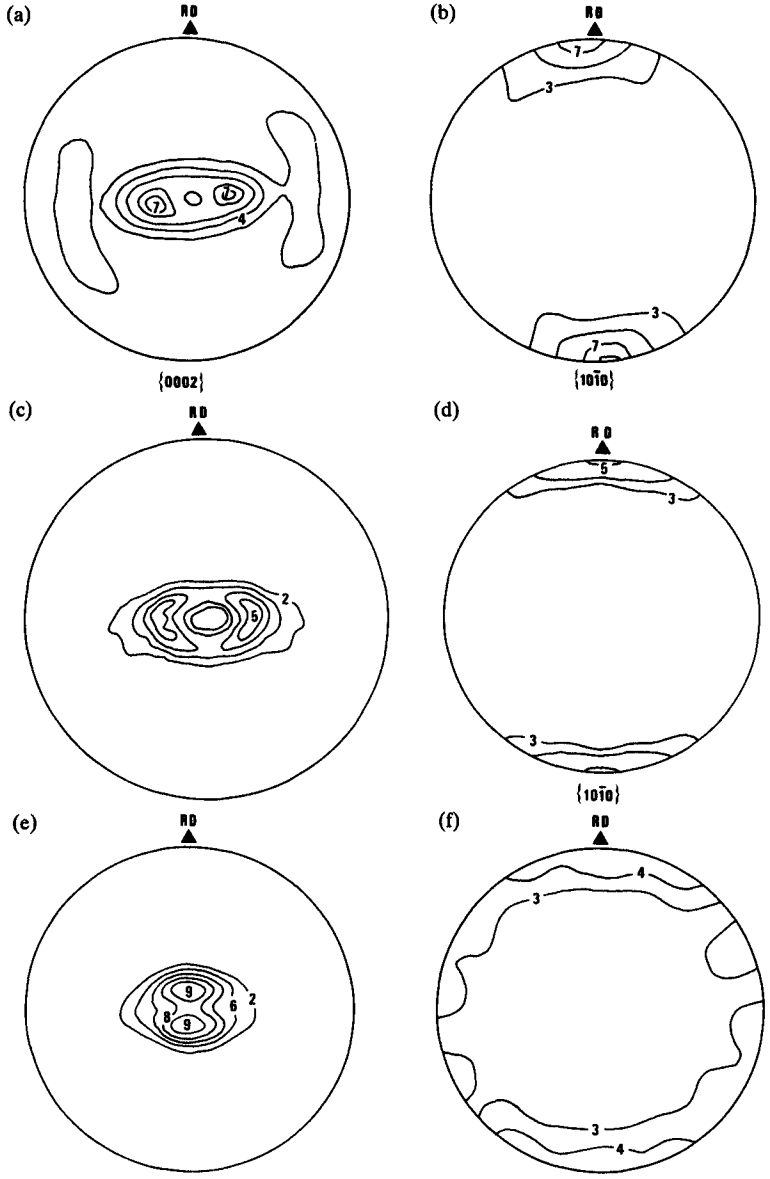

Figure 1 Pole figures {0002} and {10$\bar{1}$0} after 50% cold rolling for T 35 (a, b), T 25O_2 4Fe (c, d), Z 25O_2 3Fe (e, f).

a completely different texture with the c-axes inclined 10°–15° towards RD. The corresponding $\{10\bar{1}0\}$-poles are distributed nearly at random, with a slight preference for RD.

After annealing, the grain size of the samples was about 40–50 μm except for those with higher Fe-content. In the latter case, grain sizes decreased to about 20 μm. The annealing textures of the samples with c-axis tilted towards TD are similar to the corresponding rolling textures, though they have weaker intensities.

For the Ti and Zr samples with high oxygen content, the c-axes are closer to ND after annealing.

After 10% stretching, the major characteristic is an alignment of the $\langle 10\bar{1}0\rangle$ axes in the direction of tension, whatever this direction. The samples stretched in the RD show a fiber texture with $\langle 10\bar{1}0\rangle$//RD (axis of tension), the c-axes spreading over a range of about 0° to 60° from ND (Figure 2). The Zr samples with high O_2-content almost do not show this fiber.

When the tensile samples are cut parallel to TD, the {0002}-PF remains almost unchanged during stretching. In all samples but $Z25O_24Fe$, the a-axes rotate towards the tensile axis. In the $Z25O_24Fe$ samples this tendency is much weaker.

In biaxial expansion, the c-axes of the Ti samples (except those with higher O_2-content) tend to build up a fiber with ND as the axis, but with a tilt angle smaller than with the initial material. Moreover, several other peaks appear at 65° from DN. The latter appear neither in the Ti with high O_2-content, nor in the Zr samples (Figure 3).

Microstructures

The Ti samples (except those with high O_2-content) show twinning. We have many twins in the samples deformed by rolling up to 50% of deformation (afterwards twins can hardly be recognized), or by biaxial expansion (Figure 4), whereas twinning is less frequent in the samples deformed by uniaxial tension. Twins of the type $\{11\bar{2}2\}$ and $\{10\bar{1}2\}$ appear in the samples stretched parallel to the RD, whereas $\{10\bar{1}2\}$ twins appear mostly in those stretched parallel to TD (Mullins and Patchett, 1981). The Ti samples with high O_2-content and Zr show only a few $\{10\bar{1}2\}$ twins. Conversely no twinning appears in the Zr samples with high O_2-content when

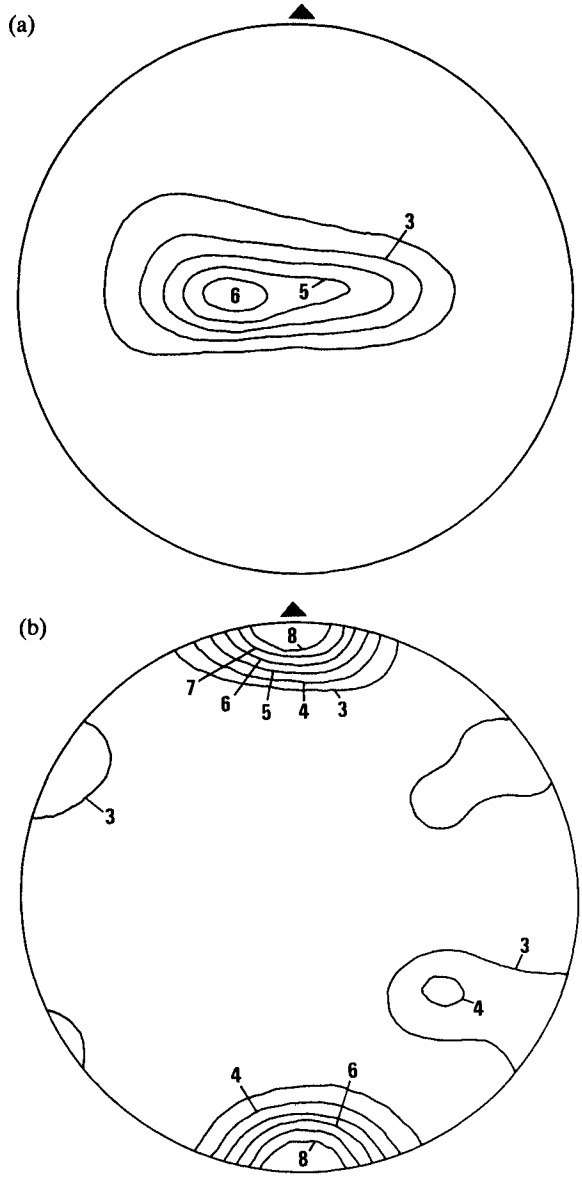

Figure 2 Pole figures {0002} and {10$\bar{1}$0} after 10% stretching in rolling direction Type II texture (a, b); in transverse direction type III texture (c, d).

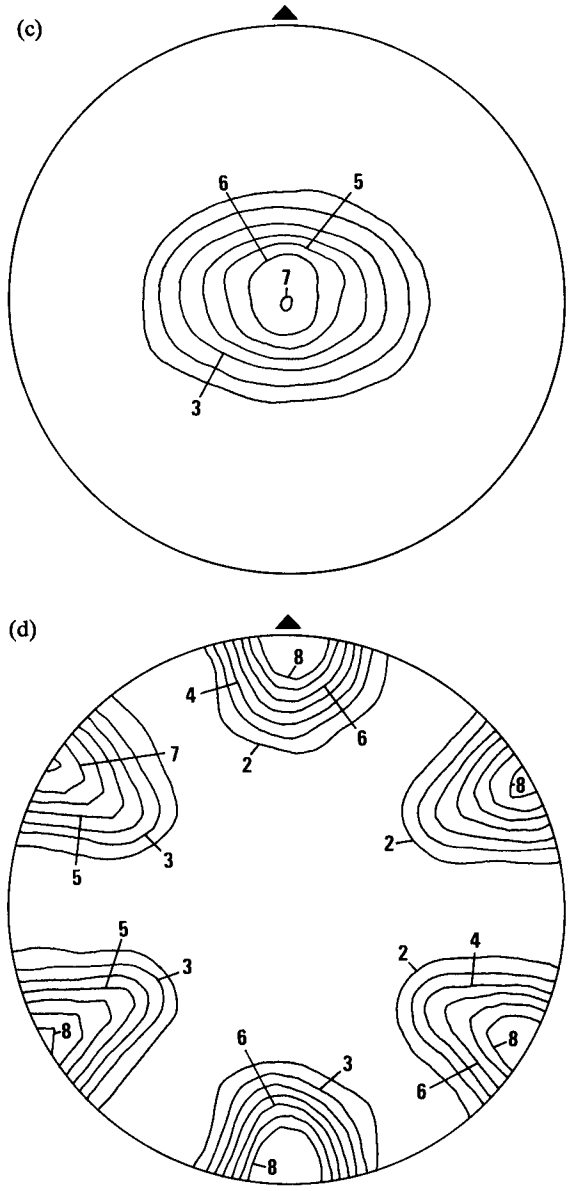

Figure 2 (*Contd.*)

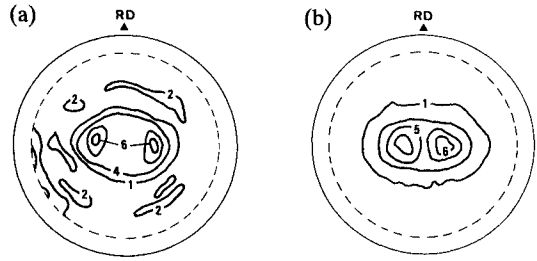

Figure 3 Pole figures {0002} measured in reflexion up to 75° after deformation in biaxial expansion for T 35 (a) Zr QN (b).

being examined under the optical microscope. But a closer examination with the TEM reveals many micro-twins near the grain boundaries.

Mechanical properties

Mechanical properties such as yield stress, maximal stress, uniform elongation at fracture are summarized in Tables 3a,b. It should be

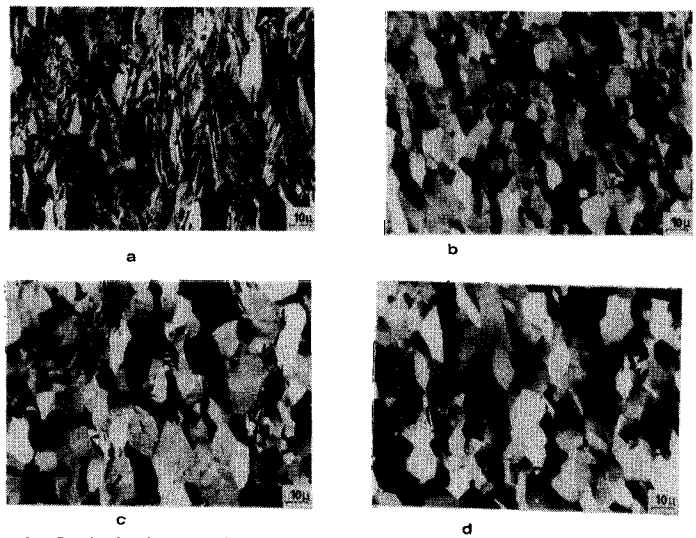

Figure 4 Optical micrography with polarized light for a) Titanium T 35 deformed in biaxial expansion at room temperature, b) Zirconium Zr QN deformed in biaxial expansion at room temperature, c) Titanium T 35 deformed in biaxial expansion at 175°C, d) Zirconium Zr QN deformed in biaxial expansion at 175°C.

Table 3a Results of the tensile test as function of the impurity level for Titanium

Denomination	e_t%		e_u%		Re (daN/mm^2)		Rm (daN/mm^2)		H_V (500)
	RD	TD	RD	TD	RD	TD	RD	TD	
$T5O_2$	52.1	47.1	26.4	12.5	18.6	25.4	33.6	32.5	120
$T8O_2$	41	39.8	12.9	11.6	25.5	32.2	39.4	38.6	145
$T5O_2$ 3Fe	53.9	44.9	34.7	21.2	17.7	26.6	32.1	32.5	112
$T9O_2$ 4Fe	48.8	49.4	26	14	28.9	34	38.2	35	130
$T18O_2$ 4Fe	37.1	35.4	16.7	12.6	39.5	43.8	48.9	47.3	117
$T25O_2$ 4Fe	33.7	36.5	15.5	13.4	43.8	46.6	53.4	52.5	206
$T9O_2$ 7Fe	47.7	46.9	25.6	14.7	28.1	33.6	38.2	35.3	134
$T9O_2$ 10Fe	48.3	53.8	26.5	14.9	27.5	32.8	38.3	35.3	134
$T9O_2$ Fe $1N_2$	37.8	39.6	18.7	12.1	33.3	39	44.3	42.7	162
$T9O_2$ 4Fe $3N_2$	39.5	41.8	20	11.2	29.7	35.8	41.8	40.1	151

e_t: total elongation, e_u: uniform elongation, R_e: yield stress, R_m: maximal stress, H_v: Vickers hardness.

noticed that an addition of iron does not impair the mechanical properties whereas the addition of oxygen, a hardening element, lowers ductility. Tables 4 and 5 show respectively Lankford's anisotropy ratio and the hardening coefficients calculated on the basis of a Hollomon type relation. Within a same series of sheets doped with oxygen the anisotropy ratio increases whereas the planar anisotropy lowers with an increasing rate of oxygen.

Table 3b Results of the tensile test as function of the impurity level for Zirconium

Denomination	e_t%		e_u%		Re (daN/mm^2)		Rm (daN/mm^2)		H_V (500)
	RD	TD	RD	TD	RD	TD	RD	TD	
$Z3O_2$	58.8	58.8	39.6	16.2	11.3	16.3	27.1	23.9	101
$Z8O_2$	53.6	48.5	28.4	14.4	17.1	21.7	31.2	29.7	128
$Z5O_2$ 3Fe	53.4	49.3	28.4	13.8	14.9	20.1	30.1	27.8	114
$Z9O_2$ 4Fe	44.3	38.1	18	13.5	27.3	31.1	37.5	36.9	146
$Z18O_2$ 4Fe	35.9	36.5	15	13.2	39.8	43.5	48.3	48.4	183
$Z25O_2$ 4Fe	33.6	33.4	13.2	12.4	52	54.4	56.7	57.1	214
$Z9O_2$ 7Fe	43.2	35.4	19.2	12.4	27.9	34.1	39.2	37.9	150
$Z9O_2$ 10Fe	41.5	38.7	19.3	13	28.7	33.8	39.5	38.5	148
$Z9O_2$ 4Fe $1N_2$	39.6	37	16.8	13.2	31.8	35.1	41.6	40.4	162
$Z9O_2$ 4Fe $3N_2$	36.2	31.4	16.4	12.3	36.4	41.9	46.3	46.5	169

e_t: total elongation, e_u: uniform elongation, R_e: yield stress, R_m: maximal stress, H_v: Vickers' hardness.

Table 4 Lankford's anisotropy ratio

Denomination	$r_0°$ RD	$r_{45°}$	$r_{90°}$ TD
$T5O_2$	2.09	3.54	4.07
$T9O_2$ 4Fe	2.27	3.23	4.10
$T18O_2$ 4Fe	2.53	3.37	4.07
$T25O_2$ 4Fe	4.16	5.26	5.63
$T9O_2$ 7Fe	2.51	3.5	4.11
$T9O_2$ 10Fe	2.56	3.58	4.22
$Z3O_2$	4.04	6.27	8.04
$Z9O_2$ 3Fe	4.58	6.32	7.77
$Z18O_2$ 3Fe	6.05	6.79	9.25
$Z25O_2$ 3Fe	5.92	5.96	5.84
$Z9O_2$ 7Fe	4.42	6.37	6.92
$Z9O_2$ 10Fe	4.75	6.13	7.93

Forming limit diagrams

The Forming Limit Diagrams (FLD) have been drawn from simulated IRSID-type tests in the two limiting cases of uniaxial tension and symmetrical biaxial expansion (Philippe, 1983) (Figures 5,6).

In uniaxial tension, the purer the titanium (or doped with Fe), the higher the $\varepsilon_1\varepsilon_2$ values. The oxygen content impairs the ductility of materials and this effect is particularly marked with Ti in biaxial

Table 5 Work hardening coefficients

Denomination	$n_{0°}$ RD	$n_{90°}$ TD
$T5O_2$	0.185	0.131
$T9O_2$ 4Fe	0.154	0.163
$T18O_2$ 4Fe	0.111	0.115
$T25O_2$ 4Fe	0.099	0.093
$T9O_2$ 7Fe	0.173	0.121
$T9O_2$ 10Fe	0.170	0.133
$Z3O_2$	0.195	0.154
$Z9O_2$ 3Fe	0.133	0.106
$Z18O_2$ 3Fe	0.094	0.089
$Z25O_2$ 3Fe	0.078	0.053
$Z9O_2$ 7Fe	0.142	0.100
$Z9O_2$ 10Fe	0.116	0.090

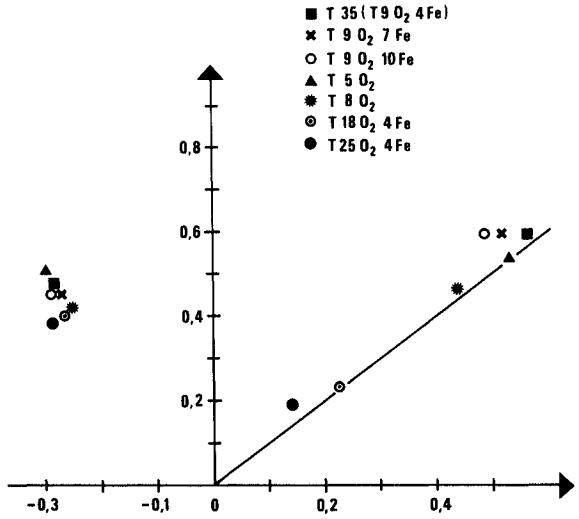

Figure 5 Forming limit diagrams at necking for Titanium of different grades at room temperature.

expansion (Philippe, 1983), where the $\varepsilon_1\varepsilon_2$ values go down rapidly with increasing O_2-level. The effect of the defomation rate and temperature on the FLD has been studied by Philippe *et al.* (1984) for Ti 35 and Zr QN. In the range of 0–200°C, the values of $\varepsilon_1\varepsilon_2$ increase with increasing temperature, except for the biaxial expansion of Ti, where the effect of temperature is just opposite (Figure 7). Moreover, the ductility of the metal in expansion is raised with an increase of deformation rate.

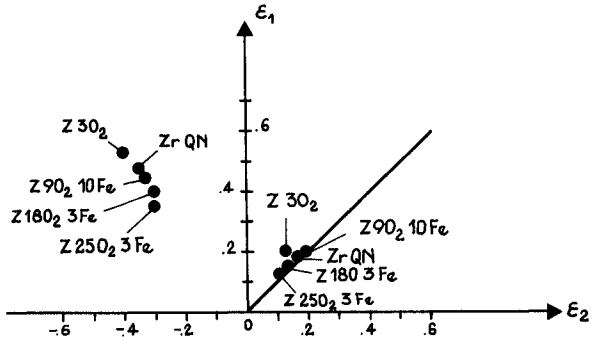

Figure 6 Forming limit diagrams at necking for Zirconium of different grades at room temperature.

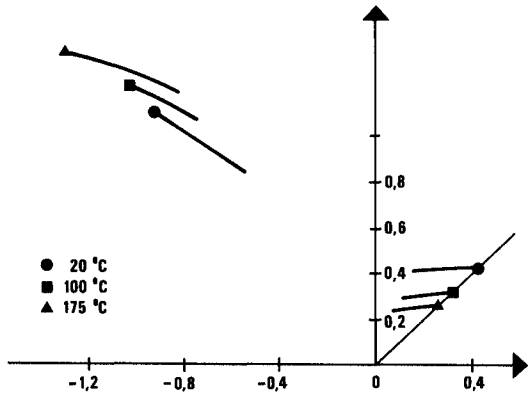

Figure 7 Influence of temperature on forming limit diagrams of Titanium (T 35).

Predeformations at low temperature

The above tests indicate that the ductility in biaxial expansion depends on the occurrence of twinning. Using predeformation of the T35 Ti samples and nuclear purity grade Zr QN at low temperature, the following points have been examined:

—evolution of the texture when the principal deformation mechanisms are twinning systems.
—the effect of the twins generated for the grade T 35 (which twins already at room temperature but practically does not at 175°C) on the later deformation at 175°C.
—the effect of the twins generated in Zr of grade QN which twins to a very limited extent at room temperature.

The operating mode of the predeformation tests are detailed in Philippe (1983) and Philippe *et al.* (1985).

A predeformation of 4% strain at −196°C weakens the major texture components. The {0002}-PFs of both Zr QN and Ti 35 undergo some spreading. Additionally, minor peaks appear at the {0002} PF periphery of only Ti 35, while a small peak appears in the central area of the corresponding $\{10\bar{1}0\}$-PF, confirming the development of minor components (Figure 8).

After 4% deformation in biaxial expansion, the Ti samples show many twins of the $\{10\bar{1}2\}$, $\{11\bar{2}1\}$ and $\{11\bar{2}2\}$ types. Conversely,

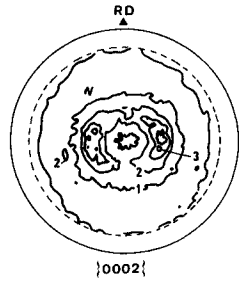

Figure 8 The {0002}-pole figure of Titanium after 4% deformation in expansion at −196°C.

twinning is much less frequent in Zr samples. The twinned volume fraction rises with increasing deformation rate, whereas it diminishes with an increasing temperature (Figure 9).

The results of the mechanical tests (predeformation at low temperature followed by biaxial expansion at 20°C or 175°C) are summarized in Tables 6a,b for the T 35 Titanium and Zr QN Zirconium grade.

First, it can be noticed that with Ti samples predeformed at low temperature and showing a high twinning rate, the later ductility at 175°C is improved to a similar or even higher level than at room temperature. Correspondingly, the micrographies (Figure 10) of the samples that were predeformed 4% at low temperature show twins after deformation at 175°C, whereas the micrographies (Figure 4) of the sample deformed directly at 175°C without predeformation do not.

Secondly, Zr samples without any trace of twinning—neither at 20°C nor at 175°C—show a better formability after predeformation at low temperature.

Finally, when the twinning ratio is too large (as, for instance, after a predeformation by rolling) the later ducitlity of the metal can be impaired.

DISCUSSION

Activation of twinning

Although no definite theory has been proposed thus far for mechanical twinning, it can now be taken for granted that two

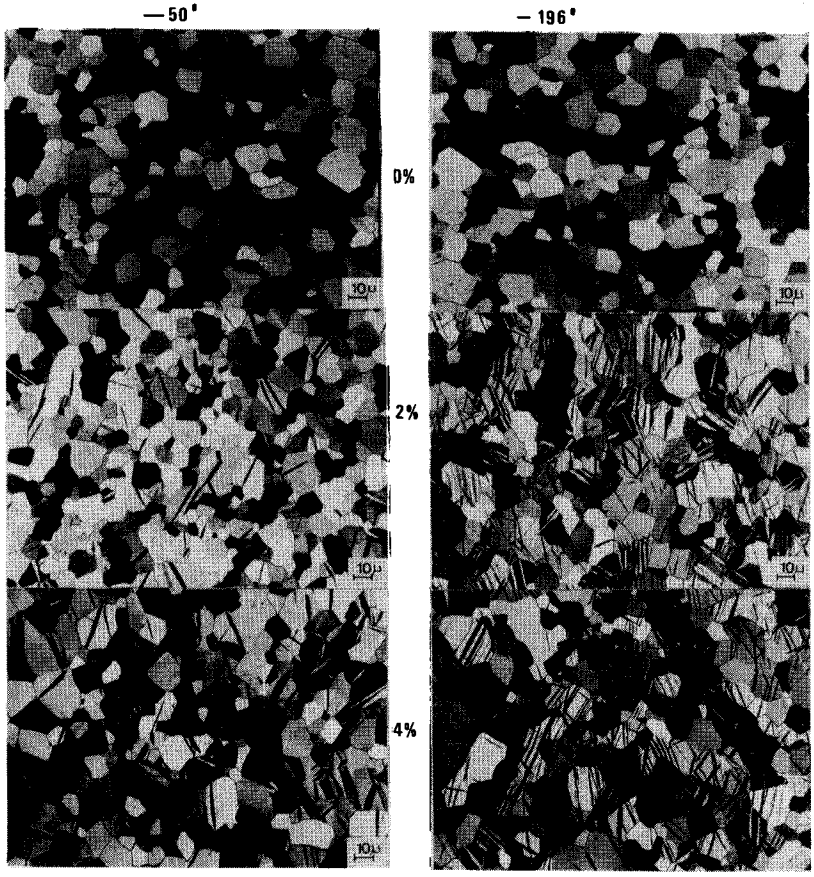

Figure 9 Influences of temperature and deformation on twinning at low temperature in Titanium T 35.

successive stages are involved:

—nucleation of the twin, (Orowan, 1965)
—growth of the twin, (Mahajan and Williams, 1973)

The addition of iron—an element of substitution—does not lessen the twinning ratio, except indirectly for some samples by reducing

Table 6a Effect of the pre-deformations on the mechanical properties of the T35 Titanium Grade.

Titanium			with pre-deformation												without pre-deformation
pre-deform. mode			Biaxial expansion								Rolling		Compression		
pre-deform. rate			2 MPa. mn^{-1}				120 MPa. mn^{-1}								
temperature of pre-deform.			−50°C		−196°C		−50°C		−196°C		−196°C		−196°C		
amount of pre deform.			2%	4%	2%	4%	2%	4%	2%	4%	9%	12%	15%	145 T	162 T	
twinned volume fraction %			20	30	60	75	30	70	80	80	70	85	100	0	5	0
final deformation ($\varepsilon 1$, $\varepsilon 2$)	20°C	necking	ε_1	0.43	0.42	0.43	0.43	0.41	0.43	0.44	0.45	0.40	0.37	0.33	0.39	0.45	0.42
			ε_2	0.33	0.33	0.34	0.36	0.34	0.32	0.34	0.36	0.32	0.30	0.27	0.33	0.36	0.31
		fracture	ε_1	0.58	0.53	0.50	0.60	0.49	0.48	0.55	0.43	0.59	0.45	0.42	0.46	0.55	0.51
			ε_2	0.52	0.47	0.50	0.54	0.43	0.2	0.50	0.42	0.49	0.42	0.36	0.44	0.51	0.45
	175°C	necking	ε_1	0.34	0.37	0.39	0.40	0.36	0.34	0.34	0.37	—	—	—	—	—	0.32
			ε_2	0.26	0.24	0.28	0.31	0.29	0.30	0.32	0.30						0.21
		fracture	ε_1	0.43	0.49	0.51	0.60	0.45	0.47	0.53	0.70	—	—	—	—	—	0.34
			ε_2	0.37	0.39	0.50	0.50	0.41	0.42	0.41	0.46						0.32

Table 6b Effect of the pre-deformations on the mechanical properties of the Zr QN Zirconium grade.

Zirconium			with pre-deformation													without pre-deformation
pre-deform. mode			Biaxial expansion								Rolling			Compression		
pre-deform. rate			2 MPa. mn^{-1}				120 MPa. mn^{-1}									
temperature of pre-deform.			−50°C		−196°C		−50°C		−196°C		−196°C			−196°C		
amount of pre deform.			2%	4%	2%	4%	2%	4%	2%	4%	9%	12%	15%	145 T	162 T	
twinned volume fraction %			3	3	5	10	0	0	5	15	5	5	5	0	0	0
final deformation (ε1, ε2) 20°C	necking	ε1	0.11	0.10	0.12	0.13	0.08	0.10	0.13	0.12	0.10	0.07	0.07	0.08	0.10	0.12
		ε2	0.04	0.04	0.07	0.07	0.04	0.05	0.06	0.08	0.05	0.03	0.04	0.02	0.05	0.05
	fracture	ε1	0.12	0.16	0.17	0.13	0.10	0.14	0.16	0.17	0.13	0.06	0.05	0.07	0.10	0.12
		ε2	0.08	0.05	0.11	0.12	0.09	0.06	0.12	0.10	0.09	0.04	0.03	0.04	0.05	0.07
175°C	necking	ε1	0.08	0.09	0.10	0.15	0.11	0.11	0.11	0.12	—	—	—	—		0.11
		ε2	0.03	0.06	0.07	0.09	0.04	0.03	0.07	0.06						0.06
	fracture	ε1	0.13	0.23	0.14	0.19	0.15	0.21	0.16	0.16						0.16
		ε2	0.09	0.19	0.12	0.17	0.10	0.11	0.14	0.14						0.12

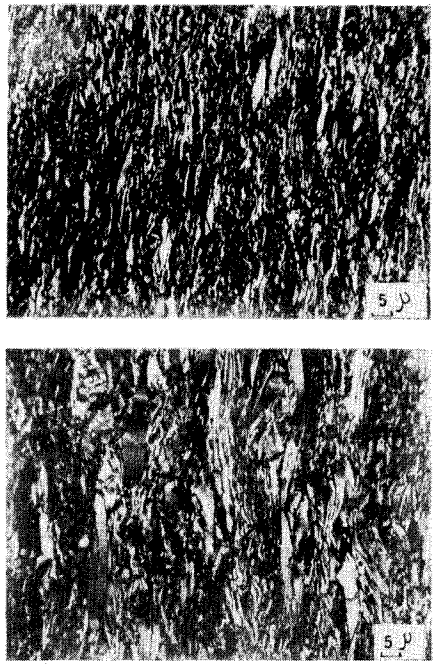

Figure 10 Optical micrographies of Titanium predeformed 4% at −196°C and deformed later at 20°C a) at 175°C b).

the grain size†. As opposed to this, the addition of oxygen—an interstitial element—markedly lessens the twinning ratio, occasionally down to zero, which is in agreement with the observations of McHargue and McCoy (1963). Moreover, the latter effect is more marked with Zr than with Ti. The micro-twins in the vicinity of grain boundaries revealed by TEM could indicate that oxygen impairs the growths of twins more than their nucleation, by hindering the mobility of the partial dislocations. When the temperature is lowered, the twins are more numerous and new types appear, which are not found at higher temperature (Partridge, 1967).

† For all the samples prepared by the authors, the grain size has been determined and taken into account in the discussion. On the contrary, the latter parameter was not always available for the results taken from the literature.

Influence of twinning on the texture

Texture of cold rolling. Rolling textures of hexagonal materials can be classified according to their c/a ratio (Wassermann and Grewen, 1962 and Dillamore and Roberts, 1965).

—Zinc and Cadmium ($c/a > 1.633$) deform by basal glide with a-Burgers vector, pyramidal glide $\{11\bar{2}2\}\ \langle 11\bar{2}\bar{3}\rangle$ with a $c+a$-Burgers vector and $\{10\bar{1}2\}$ twinning in compression, (Price 1960).

—Magnesium ($c/a = 1.633$) deforms by basal glide, $\{10\bar{1}2\}$ twinning in tension, pyramidal glide $\{11\bar{2}2\}\ \langle 11\bar{2}\bar{3}\rangle$ and, to a smaller extent, prismatic glide in some alloys, (Wonsiewich and Backofen 1967 and Kelly and Hosford 1968).

—Titanium, Zirconium and Hafnium ($c/a < 1.633$) deform by prismatic glide, pyramidal glide $\{10\bar{1}1\}\ \langle 11\bar{2}0\rangle$ with an a-Burgers vector and $\{10\bar{1}1\}\ \langle 11\bar{2}\bar{3}\rangle$ with a $c+a$-Burgers vector, $\{10\bar{1}2\}$ twinning in tension, $\{11\bar{2}2\}$ twinning in compression and, in some cases, $\{11\bar{2}1\}$ twinning in tension, (Rosi *et al.* 1956, Conrad 1981 and Chin 1975).

—Beryllium ($c/a < 1.6333$) does not deform as expected from a subnormal metal. Indeed, basal glide is the major mechanism, followed by prismatic glide and by $\{10\bar{1}2\}$ twinning in tension, (Mahajan and Williams, 1973 and Chin, 1975).

Before analysing the role of twinning in detail, it should be recalled that twinning achieves a reorientation which is usually much more important than that of gliding. Moreover, twinning in hexagonal materials is markedly polarized, some systems being only activated by tension along the c-axis, other by compression, (Yoo, 1981). Thus, in current cases of forming, e.g. drawing or rolling, where the principal components of the applied stresses are known, it is relatively easy to estimate roughly the probability for a given system to be activated. Similarly, mere geometrical considerations of lengthening or shortening of particular directions with respect to the forming process allow us to exclude some twinning systems because of the incompatibility of the final orientation that would be reached.

Geometrical considerations as above allow us to understand the

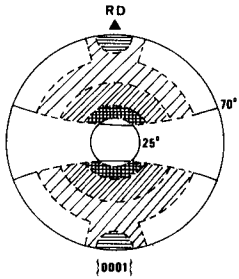

Figure 11 Theoretical pole figure {0002} for zinc after Calnan, 1951.

main features of the contribution of twinning to the texture development when forming, without resorting to elaborate models of polycrystalline plasticity, (Wassermann and Grewen, 1962).

The rolling texture of zinc has been predicted by Calnan and Clews (1951). Basal glide tends to orientate the *c*-poles in ND and the $\langle 11\bar{2}0\rangle$-axes in RD. The twin system $\{10\bar{1}2\}$ operates in compression, the *c*-poles being reorientated from the ND (compression) into RD (tension), thus explaining the emptiness in the central region as well as the secondary peak in RD for the {0002}-PF. When the $\{11\bar{2}2\}$ $\langle 11\bar{2}\bar{3}\rangle$ glide is additionally taken into consideration, the evolution of the *c*-axes PF, although rather similar, is slower (Figure 11).

Magnesium has the same glide systems as Zinc, which leads to a similar evolution of the texture by glide. Conversely, the $\{10\bar{1}2\}$ twin system operates not in compression, but in tension. The *c*-poles inside a cone of axis RD are located in the central area of the {0002}-PF after twinning and strengthen the central component (Figure 12). When pyramidal $\{11\bar{2}2\}$ glide is considered in addition, the *c*-poles tend towards RD. Prismatic glide has been evidenced in the case of hot plane strain extrusion for some particular alloys; the *c*-axes migrate then from ND towards TD (Dillamore *et al.* 1972). The orientation of the axes $\langle 10\bar{1}0\rangle$ in the case of rolling can be understood when considering cross-slip (Philippe *et al.*, 1987).

Thus, it is easy to analyse the role of the twinning in the above two cases, showing only one major twinning system each.

The corresponding task is more difficult for Ti and Zr alloys,

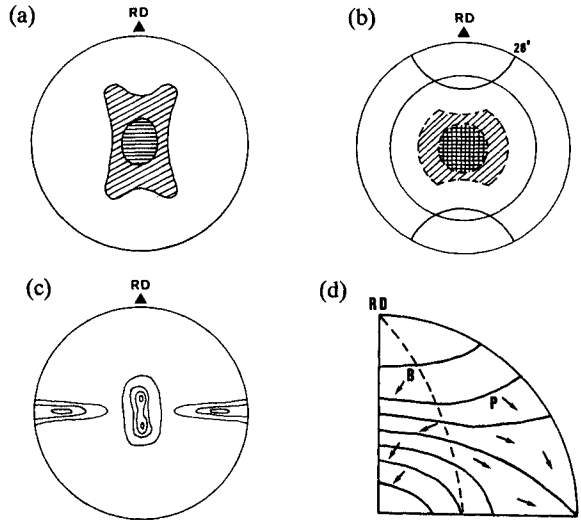

Figure 12 {0002} Pole figure for Magnesium. a) experimental after 97.5% cold rolling Calnan and Clews 1951, b) theoretical Calnan and Clews 1951, c) experimental for hot plane strain extruded Dillamore *et al.* 1972, d) theoretical Dillamore *et al.* 1972.

which show several twinning systems. A comprehensive study requires a systematic investigation in TEM.

A first attempt to explain the cold rolling texture of Ti was undertaken by Williams and Eppelsheimer (1952) and extended later on to other hexagonal materials (Eppelsheimer and Gould, 1956).

According to the authors, the $\{10\bar{1}2\}$-twinning system activated in tension empties the {0002}-PF in the vicinity of RD (up to ~28° from RD) Figure 13, whereas the $\{11\bar{2}2\}$-twinning system activated in compression empties the same PF in the central area (up to ~30° from ND). Hobson 1968 predicts the textures of Zr with *c*-axes tilted towards TD. This analysis is based upon an observation of the evolution of some specific textures and the determination of geometrical Schmid factors. The $\{10\bar{1}2\}$, $\{11\bar{2}1\}$ and $\{11\bar{2}2\}$ twinning systems that supposedly had the same critical resolved shear stress (CRSS) are taken into consideration up to third order twinning.

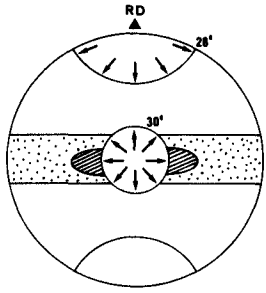

Figure 13 Theoretical {0002} pole figure for cold rolled Titanium Williams and Eppelsheimer, 1952.

In the latter two referenced works, the CRSS are not really known. Nevertheless, the major tendencies reappear. Thornburg (1971) and Thornburg and Piehler, (1975) followed the evolution of the texture of some Ti alloys rolled to various reductions. They examined the active deformation mechanisms by TEM and calculated the lattice rotations associated with various combinations of active glide systems. Thus, they obtained the classical Ti-texture with c-poles tilted towards TD by combination of several glide systems with the $\{10\bar{1}2\}$—and $\{11\bar{2}2\}$—twinning systems.

Conversely they predicted the texture with central c-poles when restricting the mechanisms to glide only. The latter texture is found in strongly rolled Ti 3%–Al (Figure 14).

Figure 15 shows the rotations of the c-poles due to the operation of various types of twinning-systems, as predicted by Tenckhoff (1978). Parallel to these calculations, this author followed experimentally, grain by grain, the reorientation associated with the various active twinning systems, up to 40% deformation. After the lattice was almost completely twinned, further twinning being blocked (Partridge, 1967).

Thus, the splitting of the c-poles in the final stable orientations tilted 20° to 40° towards TD could be accounted for by pyramidal glide with a $\langle c+a\rangle$-Burger's vector, on the $\{11\bar{2}1\}$ or $\{10\bar{1}1\}$ planes.

Lee *et al.* (1987) followed the evolution of the texture step by step when cold-rolling Ti-sheets from 0% to 80% area reduction. By means of three dimensional texture analysis, they could follow the

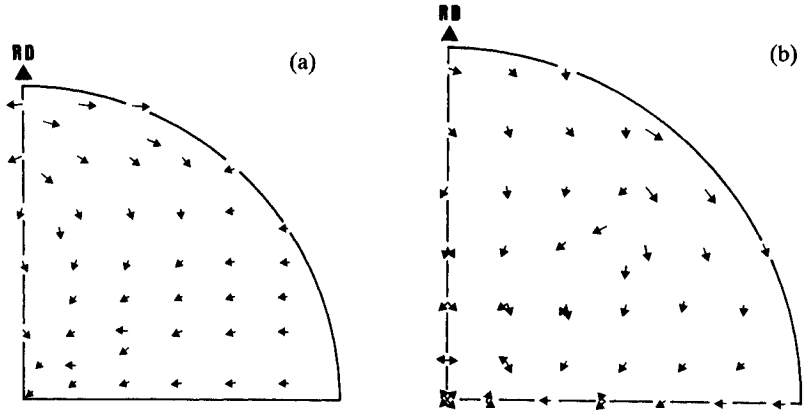

Figure 14 {0002} Pole figures for Titanium and Titanium alloys a) rotations due to only slip involved in the plane strain deformation of crystals of various orientations for an applied strain of 0.05 after Thornburg and Piehler 1973 b) Rotations due to slip involved in the plane strain deformations for an applied strain of 0.05 after Thornburg and Piehler. In addition to deformation by slip, $\{11\bar{2}2\}$ and $\{10\bar{1}2\}$ twins also operate.

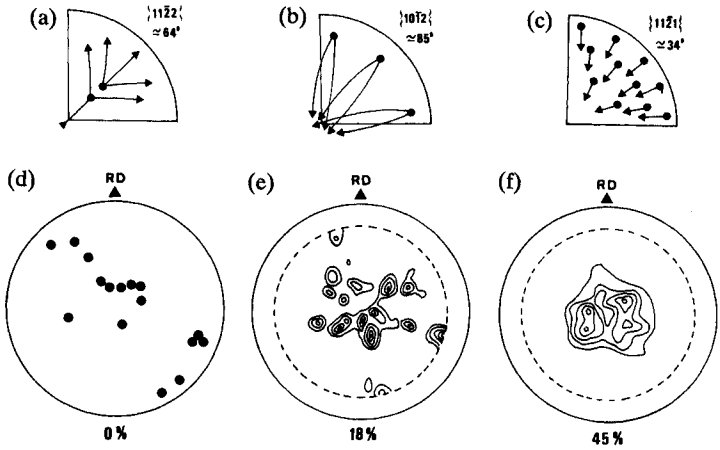

Figure 15 a,b,c) Spontaneous lattice rotations of the basal pole due to twinning in zirconium Tenckhoff 1978, d,e,f) development of the preferred alignment of basal poles (experimental) in zirconium Tenckhoff 1980.

development of even the minor components and interpret it with the operation of eligible twinning mechanisms. In particular, they could explain the stregthening or the weakening of some components by taking into consideration the marked anistropy of twinning with respect to the applied stresses (resp. tension or compression) and the deformations undergone (resp. lengthening or shortening).

In all the above mentioned works, especially the T-type textures (*c*-poles tilted towards TD) have been studied. However, other types of textures can be found in Ti and Zr alloys about which we are going to report, together with micrographic analyses, when available.

Thornburg (1971) had already mentioned a texture with central *c*-poles in Ti alloys with 2% or 3% aluminium which did not show any twins. Similar textures were determined by Hasegawa and Nishimura (1973) in Ti alloys highly doped with oxygen or aluminium. Williams and Eppelsheimer (1953) have rolled samples with increasing impurity contents and evidenced another texture component with *c*-axes tilted out of ND about 15°–20° towards RD, especially in the most heavily doped and most severely rolled samples (Figure 16). Our results corroborate these tendencies. In

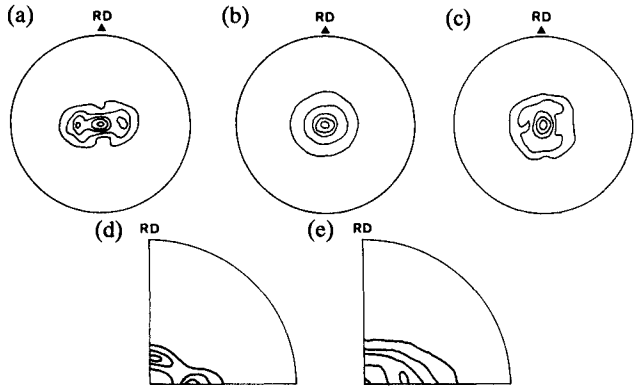

Figure 16 Experimental {0002} pole figures for Titanium and Titanium alloys. a) Titanium with high level of oxygen cold rolled Hasegawa and Nishimura 1973, b) Ti 4Al cold rolled Hasegawa and Nishimura 1973, c) Ti 5 Al 2.55 N cold rolled Hasegawa and Nishimura 1973, d) Ti with high level of metallic impurities and cold rolled 95.8% Williams and Eppelsheimer 1953, e) Ti 1.5% Al cold rolled 60% Thornburg and Piehler 1973.

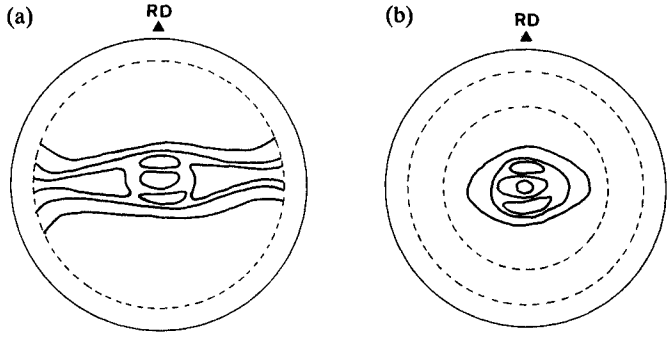

Figure 17 {0002} Pole figures for Zircaloys 2. a) cold rolled 50% Ballinger and Pelloux 1981, b) cross rolled 50% Ballinger and Pelloux 1981.

ZR with high oxygen content the two above mentioned peaks in the ND–RD plane are strongly marked and the samples do not show any twins. In Ti with high oxygen content, the peaks towards TD show a large spread drawing a belt from TD axis towards RD. Moreover, we progressively cold-rolled Zr of grade QN up to 98% and observed after 75% rolling a reorientation of the *c*-poles towards ND. The corresponding samples did hardly show any twinning, which is in compliance with the small grain size and the fair oxygen content in this Zr grade.

Finally, the (0002) PFs of several zircaloys show both series of peaks, one in the (ND-TD) plane, the other in (ND–RD), Ballinger and Pelloux (1981) (Figure 17). An extensive examination of our Zr and Zy samples by TEM led us to the conclusion that there is cross slip with a common *a*-Burgers vector from prismatic to pyramidal plane; the higher the oxygen rate, the more frequent this mechanism (Philippe *et al.*, 1988). When $\{11\bar{2}2\}$ twinning could not operate, pyramidal $\langle c + a \rangle$-glide is frequent (Philippe *et al.* 1988). Finally when rolling up to higher degrees (>60%) shear bands appear all the faster as twinning operates less.

A further and more quantitative stage of analysis can be reached with the help of polycrystal plasticity models, e.g. Taylor model, (Bunge 1970 and van Houtte and Aernoult 1975a and b). Such models allow to predict the forming textures (uniaxial stretching, wire drawing, rolling . . .) when the critical resolved shear stresses

(CRSS) are given. However, the latter are known only approximately in hexagonal materials, and they are very sensitive to the slightest alteration in impurity rates. Therefore, the values proposed in the literature call for a confirmation. In addition, the active deformation mechanisms have to be checked by optical and transmission microscopy.

Sztwiertnia *et al.*, (1985) performed Taylor type simulations of rolling textures of zinc, with a combination of $\{0001\}\ \langle 11\bar{2}0\rangle$ basal glide, $\{11\bar{2}2\}\ \langle 11\bar{2}\bar{3}\rangle$ pyramidal glide and $\{10\bar{1}2\}\ \langle 11\bar{2}\bar{3}\rangle$ compression twinning.

We have made Taylor simulations of the rolling texture of Ti and Zr alloys, guided by the evolution of the texture in samples rolled to an increasing degree on one hand, and on extensive micrographic studies in optical and electronic microscopy on the other hand.

The combination of $\{10\bar{1}0\}\ \langle 11\bar{2}0\rangle$ and $\{10\bar{1}1\}\ \langle 11\bar{2}0\rangle$ glides and $\{10\bar{1}2\}\ \langle 10\bar{1}1\rangle$ tension twinning and $\{11\bar{2}2\}\ \langle 11\bar{2}\bar{3}\rangle$ compression twinning leads to T-type textures (c-poles tilted towards TD). The combination of $\{10\bar{1}0\}\ \langle 11\bar{2}0\rangle$ prismatic glide, $\{10\bar{1}1\}\ \langle 11\bar{2}0\rangle$ and $\{10\bar{1}1\}\ \langle 11\bar{2}\bar{3}\rangle$ pyramidal glide and $\{10\bar{1}2\}\ \langle 10\bar{1}\bar{1}\rangle$ twinning the latter being strongly impaired leads to R-type textures (c-poles tilted about 15°–20° from ND towards RD) (Figure 18).

The addition of possible basal glide to the combination of deformation mechanisms orientates the c-axes closer to ND.

After 50% deformation, it becomes rather uneasy to make reliable determination of the deformation mechanisms which were active. Anyhow, the development of twins is rather unlikely at such high deformation, (Tenckhoff 1980 and Nauer-Gerhardt 1987). Alloys which do not twin at all and which have their c-poles in ND, will most probably deform further by gliding. The $\langle c+a\rangle$-gliding is confined, at high deformations, to bands close to $\{11\bar{2}\bar{4}\}$, as reported by Jensen and Backofen (1972). The orientation of the latter planes is in fair agreement with the orientation of the shear bands—making an angle of about 35° with the sheet plane—in the sheets under consideration having the c-axes tilted about 15° from ND towards RD (Figure 19). In alloys twinning slightly, $\langle c+a\rangle$-pyramidal glide has to take place and the c-axes become thus closer to ND or even rotate towards the plane (ND, RD).

Finally, in alloys twinning extensively (e.g. Ti with low oxygen content), the c-poles remain in the plane (ND, TD).

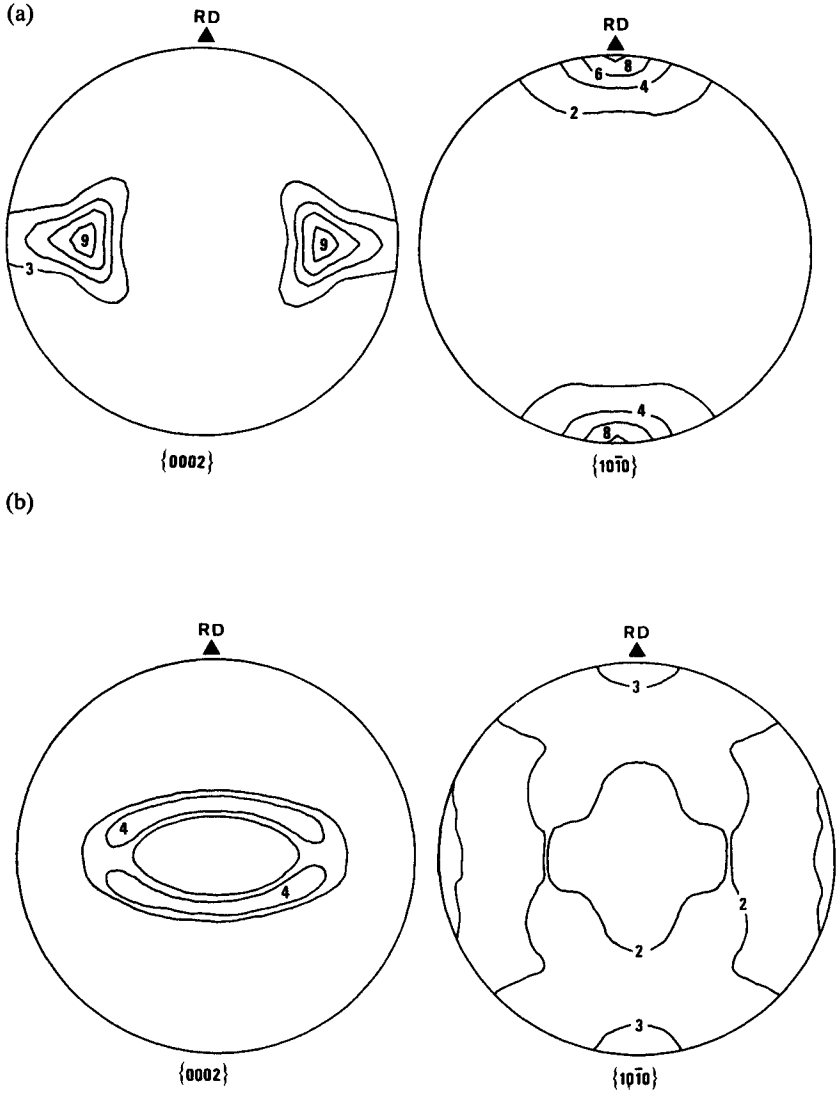

Figure 18 Theoretical Pole figures for Titanium and Zirconium. a) with prismatic glide, pyramidal $\langle a \rangle$-glide and $\{10\bar{1}2\}$, $\{11\bar{2}2\}$ twinning, b) with prismatic glide, pyramidal $\langle a \rangle$-glide, pyramidal-$\langle c+a \rangle$ glide and $\{10\bar{1}2\}$ twinning.

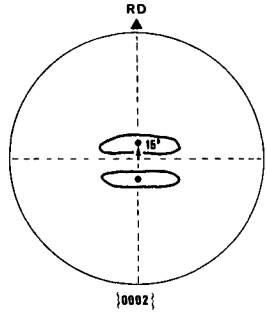

Figure 19 Position of c-axes on the {0002} Pole figure with shear banding on $\{11\bar{2}\bar{4}\}$ plane (a-axes are in RD).

It should be emphasized that the latter textures remain stable during annealing, contrary to all above mentioned textures which tend to c-type textures (c-poles central). Under these circumstances, it is hard to decide whether these Ti samples go on twinning with increasing deformation, the microstructures being already twinned. On the other hand, it seems reasonable that cross-slip with a $\langle 11\bar{2}0\rangle$ Burgers vector on $\{10\bar{1}1\}$ and {0002} planes becomes the more active the higher the deformation degree. Indeed, it can be shown that this texture remains stable under the operation of the glide systems $\{10\bar{1}0\}$, $\{10\bar{1}1\}$ and {0002} having a common $\langle a\rangle$ Burgers vector and $\{10\bar{1}1\}$ having $\langle c+a\rangle$ Burgers vector.

Deformation textures. In uniaxial stretching, twinning is hardly activated up to 10% deformation. The progressive reorientation of the $\langle 10\bar{1}0\rangle$-axes parallel to tensile axis is essentially due to gliding (Philippe *et al.* 1987).

In biaxial expansion of Ti alloys with low oxygen content (<800 ppm O_2 in weight), twinning operates to a large extent and the minor components which appear in the texture are in twin relation with the major components, according to the $\{11\bar{2}2\}$ $\langle 11\bar{2}\bar{3}\rangle$ systems. Twins of the latter type are actually observed in large numbers in samples which have been deformed by the bulge test. In this test, the c-axes close to ND are stressed in compression

as required for the activation of the $\{11\bar{2}2\}\ \langle 11\bar{2}\bar{3}\rangle$ systems, whereas all the directions in the sheet plane are stretched. Otherwise, in alloys which hardly ever twin, the $\{11\bar{2}2\}$ type twins can practically not be evidenced and the minor components do not appear either. In all bulge tests, the *c*-axes show a tendency to build a partial fiber component with fiber axis ND (see above § Rolling Texture and Texture Development by Tension or Biaxial Expansion) which is consistent with either the gliding systems and the axial symmetry presented by the test.

Effect of twinning on the yield loci

The yield limit Re varies within a large range according to the stretching direction (tension in RD resp. TD) in all the alloys but those twinning hardly. In the latter cases, the alloys show textures of the *c*-type (central *c*-poles) with quasi isotropic distribution of *a*-axes in the sheet plane, leading to a higher planar isotropy.

Twinning introduces a marked anisotropy in the yield loci, especially when restricted to a unique system, as in Mg (Kelly and Hosford 1968) (Figure 20). Indeed, this figure shows a higher strength in tension than compression at 1% and even 5% deformation. According to the particular texture under consideration, compression (about orthogonal to *c*-axes) results in a tension (about parallel to *c*-axes) which easily activates the $\{10\bar{1}2\}$ tension twin. In the opposite view, tension (about orthogonal to *c*-axes) results in a compression (about parallel to *c*-axes) contrary to the $\{10\bar{1}2\}$ tension twin, and the basal glide cannot operate either. The dissymetry is lessened in Mg4Li alloys by additional operation of prismatic glide. But in all hexagonal metals deforming by a restricted number of glide and twinning systems, the sharper their texture, the more marked is the dissymetry (Burgraff and Wincierz 1981, Ballinger and Pelloux 1981). Several authors have modelized the yield loci of samples with sharp texture to obtain a better understanding of the active deformation mechanisms.

Moreover, in metals deforming preferentially by twinning, the yield stress increases with increasing temperature and decreases with increasing deformation degree. This is notably the case when deforming Ti in compression, accommodating preferentially by $\{11\bar{2}2\}$ twinning (Reed-Hill 1971).

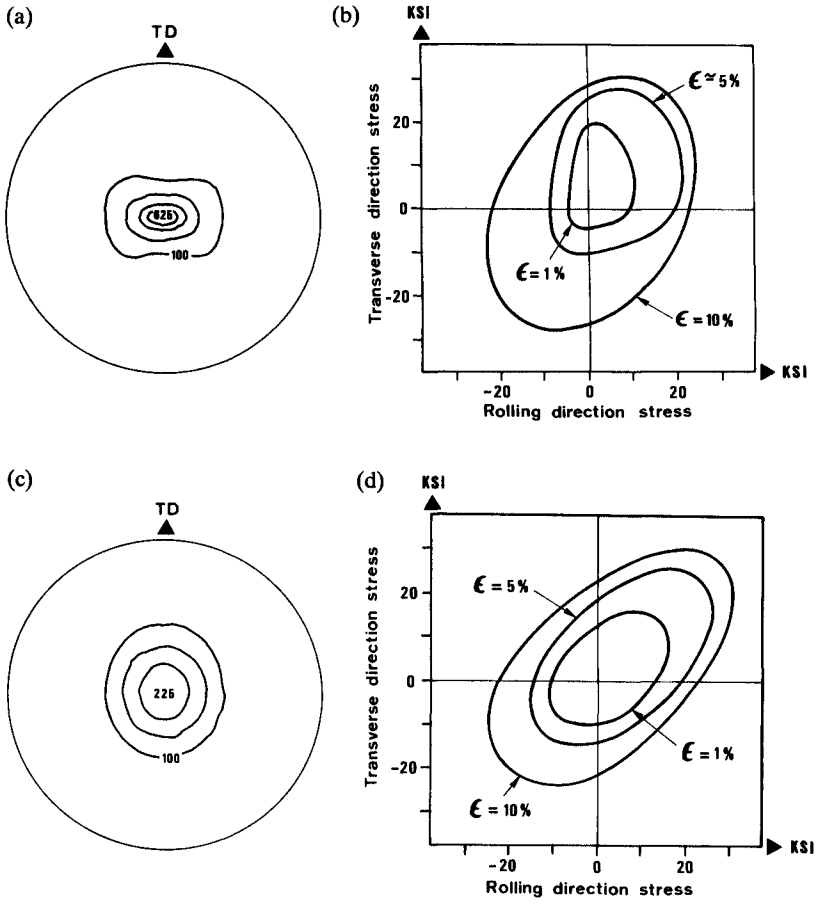

Figure 20 Texture and yield loci after Kelly and Hosford for pure Magnesium (a,b) for Mg4%Li alloy (c,d).

Twinning and mechanical properties

Kelly and Hosford (1968), Conrad (1981) and Reed-Hill (1971) have evidenced basic differences between the σ, ε curves in stretching and the corresponding curves in compression. According to the textures of the samples, they could put these differences down to behaviour of the monocrystal.

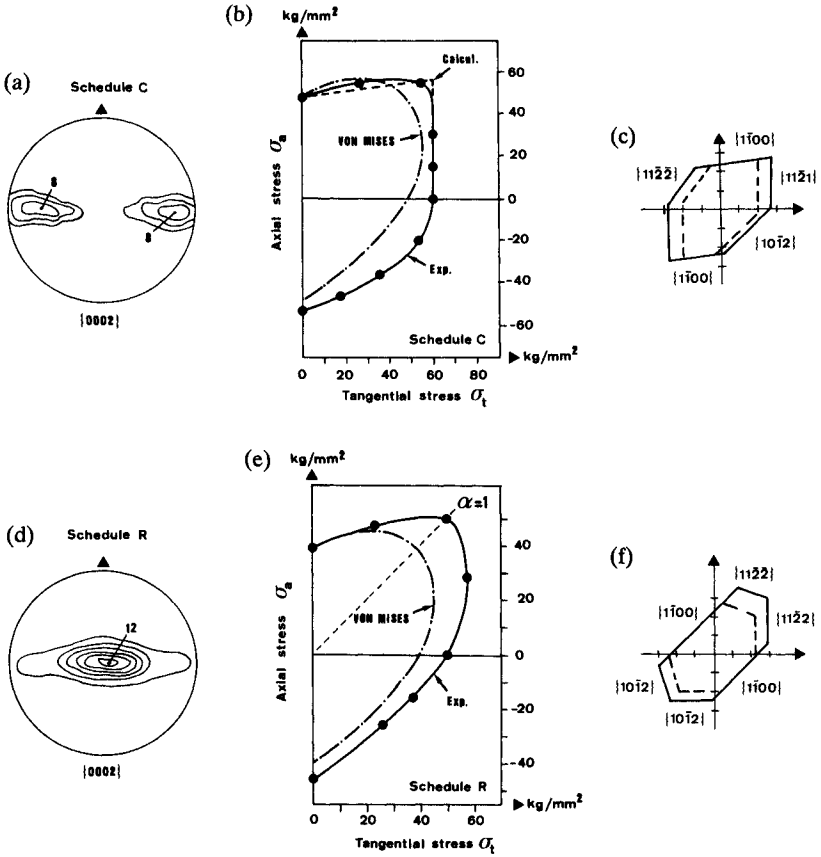

Figure 21 Texture, experimental yield loci and recalculated yield loci for 2 schedules of Zy 4 with different initial textures Dressler *et al.* 1972.

Indeed, as inferred just above, samples stressed in compression undergo a tension along the *c*-axes and the $\{10\bar{1}2\}$ twinning cannot operate (neither can the basal glide), whereas when stressed in compression, the $\{10\bar{1}2\}$ twinning is activated (Figure 22).

Many authors reported an improvement of ductility when twinning operates. This is notably the case in Ti Iodide (Reed-Hill, 1971) (Figure 23) and in Zr, where a lowering in temperature yields an increase in twinned volume fraction, in the uniform elongation

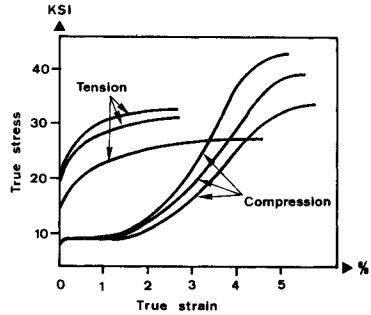

Figure 22 Stress-strain curves of Polycristalline magnesium rod with a strong fiber texture. The difference in the compressive and tensile curves is due to the $\{10\bar{1}2\}$ twinning that occurs in compression (quoted in Reed-Hill 1971).

and in the total elongation. Similarly, the combination of gliding and twinning results in an increase of the hardening rate (Dabosi, 1975).

This effect is illustrated by a more detailed comparison between Ti and Zr. At higher temperatures (about 150°C) where neither Zr nor Ti twin, samples with similar textures show rather similar stress-strain curves (Reed-Hill, 1972). At lower temperatures

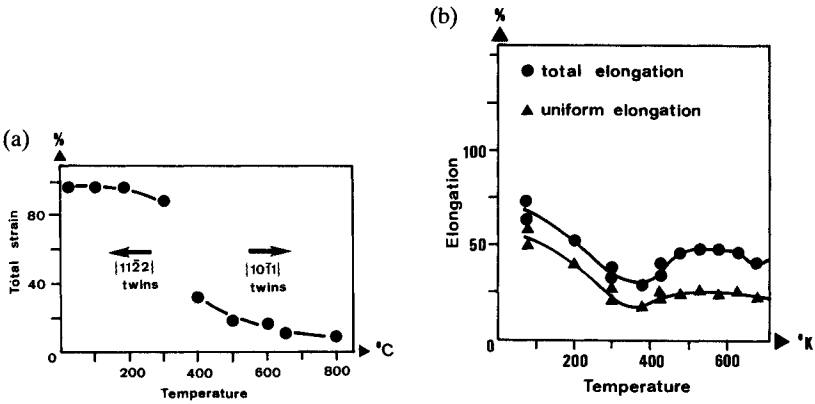

Figure 23 Influence of twinning on ductility of Titanium (quoted in Reed-Hill 1971). a) titanium crystals compressed to the basal plane. b) Uniform and total elongation of high purity titanium.

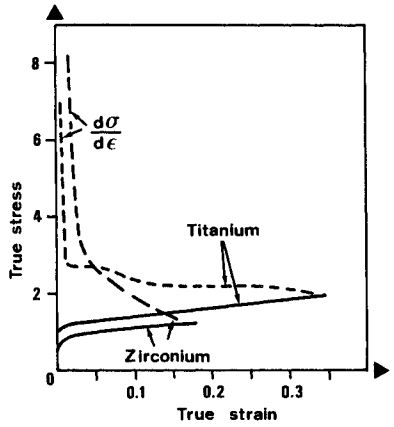

Figure 24 Stress-strain curves of longitudinal zirconium and titanium specimens at 77°K after Reed-Hill (1972).

(77°K), whereas in Zr the work hardening ratio $d\sigma/d\varepsilon$ drops continuously with the deformation, it remains constant in Ti for strains greater than 2% (Figure 24), thus producing a very large uniform elongation (Mullins and Patchett 1981).

Garde *et al.* (1973) explain such a hardening by either geometrical factors (twin orientation more or less favourable to further glide) or by microstructures (subdivision of grains by twin boundaries).

In the early stages of the deformation, these effects are weak, and the effect of twinning on hardening (small diminution of $d\sigma/d\varepsilon$) is due initially to a deformation increment without significant stress increment, according to:

$$d\sigma/d\varepsilon = d\sigma/(d\varepsilon_T + d\varepsilon_G)$$

where $d\varepsilon_T$ is the contribution of twinning and $d\varepsilon_G$ that of gliding to the deformation (Vöhringer, 1969).

In the later stages of deformation Ti shows a microstructure with many twins, whereas Zr shows only a few large twins. After 1% deformation, the high values of the hardening ratio of Ti can be explained by structural hardening associated to the subdivision of the microstructure and by interactions between twins and dislocations as shown by Yoo (1981).

Our tests corroborate these statements (Phillipe, 1983). However,

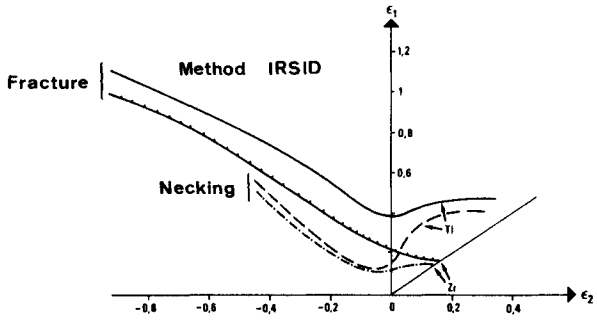

Figure 25 Forming limit diagrams for T 35 and Zr QN at room temperature.

according to the texture of our samples, it is especially interesting to study them in the bulge test. Indeed, the easy glide systems are not sollicited then due to their unfavorable orientation, and twinning systems have to contribute to accommodation.

Twinning and forming

A comparison of FLD for Ti (T 35) and Zr (QN) (Figure 25) shows that the behaviour of both materials is comparable in stretching but rather different in biaxial expansion (Philippe *et al.*, 1984). In uniaxial stretching, the prismatic glide which is the easy glide in both metals contributes widely to accommodating the deformation. In biaxial expansion, the easy glide systems are impaired by small geometrical (Schmid) factors according to the crystallographic texture of the samples. The latter glide systems have thus to be replaced to a large extent by $\{11\bar{2}2\}$ twinning and $\langle c+a \rangle$ gliding. When deforming at room temperature in the bulge test, Ti shows a great many $\{11\bar{2}2\}$ twins (Figure 4) whereas Zr does only a few. As pyramidal $\langle c+a \rangle$ glide is difficult, fracture occurs early in the latter material.

When deforming at different temperatures and rates, the above conclusions are confirmed. Indeed, when accommodation is achieved essentially by glide, an increase in the deformation temperature improves the ductility.

Conversely, when twinning contributes to a large extent to

accommodation, an increase in the deformation temperature weakens the ductility. This occurs notably in Ti deformed at 175°C and above, when both twinned volume fraction and ductility are lowered (Figure 7).

The bulge tests applied to doped samples indicate that only samples which include twins show a good ductility in biaxial expansion. This behaviour is still strengthened by the textures of the samples undergoing twinning. Indeed, the twins present geometrical (Schmid) factors for easy glide which are distinctly improved as against the matrix. Most samples which do not twin show an annealing texture with central c-poles, and the orientation (Schmid) factors almost vanish.

When predeformed at low temperature in biaxial expansion Zr contains enough twins to improve further formability of the material at room temperature or at 175°C.

After a 4% predeformation at −196°C, Ti contains enough twins to offer at 175°C a ductility comparable to that which it had at room temperature, though the ductility of Ti at high temperature is considered to be rather poor. In the latter case, however, the twinned volume fraction is smaller than after deformation at room temperature. At the stage of predeformation at low temperature, in addition to the current twin types $\{10\bar{1}2\}$ and $\{11\bar{2}2\}$, the particular twins of type $\{11\bar{2}1\}$ become active. The latter twins are characterized by an important twin-shear (~0.6) and thus contribute much to accommodation. Moreover, predeformation at low temperature may have introduced twin nuclei which grow up at the time of final deformation.

However, too severe a predeformation at low temperature (e.g. by rolling) may slightly lower the ductility in expansion, in spite of a high twinning rate. This can be understood by the following considerations:

—first, a very high twinning rate may induce local stress concentrations which sometimes hinder nucleation of further twins or even give rise to micro-cracks;

—secondly, when the final deformation mode is different from the initial predeformation mode, the twins generated in the final deformation are of a different type, too, and might build up barriers hindering the further glide of dislocations.

Thus, when a material has a limited number of deformation mechanisms and marked preferential orientations (i.e. marked texture), the ductility of the material may vary to a great extent according to the type and direction of the sollicitations. Sheets having a sufficiently high number of available deformation mechanisms to be activated for plastic accommodation show both a good ductility in stretching and a good formality. Our experience is that the latter sheets showed mean r-values in any direction ranging from 0.8 to 4 and yield loci that are neither too dissymetrical nor too excentred in their shape. In Ti and Zr alloys, the corresponding textures were of the transverse type, with a rather large tilt angle of the c-axes, thus allowing an easy accommodation of compression by $\{11\bar{2}2\}$ twinning.

When the $\{11\bar{2}2\}$-twinning cannot accommodate the compression along the c-axis, it should be replaced by the pyramidal $\langle c+a\rangle$-glide. If the latter is difficult as in Zr (extremal r values, yield loci with marked ellipticity), the ductility is much poorer in expansion than it was in traction when accommodation occurred by prismatic and cross slip. Moreover, these alloys show a strong central texture (c-poles in the vicinity of ND).

Contrarily, the forming limit diagrams of a ZnCuTi alloy (Engineering Properties of Zinc Alloys, 1981) show a good ductility in expansion, whereas it is poorer in tension, the difference being founded as previously on the difference in the accommodating deformation mechanisms.

Thus, for such hexagonal materials, ductility in expansion can hardly be inferred from ductility in stretching, and *vice versa.*

CONCLUSION

This work reviews the conditions for activation of twinning and its effect on the evolution of the textures in hexagonal materials.

It also proves that the modelization of polycrystalline plasticity and texture evolution in hexagonal materials requires an extensive study of the active glide and twinning systems by T.E.M., taking into account the anisotropy and polarization of the possible twinning systems.

Hexagonal materials show severe textures and their ductility

depends strongly on the deformation mode, according to the glide and twinning systems able to perform accommodation.

Acknowledgments

The authors express their gratitude to R. Tricot and D. Charquet (CEZUS) and to J. Decours (CEA Saclay) for their technical assistance in the preparation and the thermomechanical treatment of the sheets. Two of them (M. J. Philippe and C. Esling) are also indebted to Prof. H. J. Bunge and to Dr. C. Nauer-Gerhardt for valuable discussions during a stay at the Institut of Metallkunde und Metallphysik der T. U. Clausthal.

References

Ballinger, R. G. and Pelloux, R. M. (1981). *J. of Nuclear Materials,* **97,** 231.
Bishop, J. F. W. and Hill, R. (1951a). *Phil. Mag,* **42,** 414.
Bishop, J. F. W and Hill, R. (1951b). *Phil. Mag,* **45,** 1298.
Bunge, J. H. (1970) *Kristall und Technik,* **5,** 145.
Burgraff, J. and Wincierz, P. (1981) *Z. Metallkde,* **72,** 287.
Calnan, E. A. and Clews, C. J. B. (1951) *Phil. Mag,* **42,** 919.
Chin, G. Y. (1975) *Metal Trans.* **6A,** 238.
Conrad, H. (1981) *Progress in Materials Sciences,* **26,** N° 24, 199.
Dabosi, F. (1975) Rapport CEZUS.
Dillamore, I. L. and Roberts, W. T. (1965) *Metallurgical Reviews,* **10,** 271.
Dillamore, I. L., Hadden, P. and Stratford, D. J. (1972) *Texture,* **1,** 17.
Dressler, G., Matucha, K. H. and Wincierz, P. (1972) *Canad. Met. Quart.,* **11,** 177.
Dressler, G., Matucha, K. H. and Wincierz, P. (1973). Proc. 2° Int. Conf. on Structural Mechan. reactor Technology Berlin.
Engineering Properties of Zinc Alloys (Int Lead Zinc Research Organisation N.Y. 68, 1981).
Eppelsheimer, D. S. and Gould, D. S. (1956). *Nature,* **177,** 241.
Garde, A. M., Altinger, E., Reed-Hill, R. E. (1973). *Met. Trans.* **4A,** 2461.
Groves, G. W. and Kelly, A. (1963). *Phil. Mag,* **8,** 877.
Guillaume, M. J., Vincent, A., Beauvais, C. and Hocheid, B. (1981). *Mem. Scient. Rev. Met.* **78,** 189.
McHargue, C. J. and McCoy, H. E. (1963). *Trans. Met. Soc. AIME,* **227,** 1170.
Hasegawa, A. and Nishimura, T. (1973). *Mat. Scien. and Tech.,* Vol. 2 Plenum Press 1349.
Hobson, D. O. (1968). *Trans. Met. AIME,* **242,** 1105.
Jensen, J. A. and Backofen, W. A. (1972). *Canad. Met. Quat.,* **11,** 39.
Kelly, E. N. and Hosford. W. F. Jr (1968a). *Trans. Met. Soc. AIME,* **242,** 654.
Kelly, E. W. and Hosford, W. F. Jr (1968b). *Trans. Met. Soc.,* **242,** 5.
Keshavan, M. K., Sargent, G. and Conrad, H. (1975). *Met. Trans.,* **64,** 1291.
Lee, H. P., Esling, C. and Bunge, H. J. (1987). In print, *Texture and Microstructure.*
Mahajan, S. and Williams, D. F. (1973). *Inst. Met. Reviews,* **16.**
Mullins, S. and Patchett, B. M. (1981). *Met. Trans.* **12A,** 853.
Nauer-Gerhardt, C. (1987). Univ. Clausthal, private communication.
Nomakura, H., Minonishi, Y. and Koiwa, K. (1986). *Scripta Met.,* **20,** 1581.
Orowan, E. (1965). *Dislocatons in Metals,* AIME New York, **116.**

Partridge, P. G. (1967a). *Metallurgical Reviews.* **12,** 169.
Partridge, P. G. (1967b). *Metallurgical Reviews,* N° 118, 169.
Philippe, M. J. (1983). Thesis, University of Metz.
Philippe, M. J., Baudet, C. and Hocheid, B. (1982) *Mem. Scient. Rev. Met.* **10,** 420.
Philippe, M. J., Esling, C. and Hocheid, B. (1984a). *Mem. Scient. Rev. Met.,* **2,** 71.
Philippe, M. J., Esling, C. and Hocheid, B. (1984b). Proc. of the 7th Icotom, Noordwijkerhout, edited by Brakman, C. M. Jongenburger, P. and Mittemeijer, E. J. 519.
Philippe, M. J., Lemoisson, P., Hocheid, B. and Fidelle, J. P. (1985). *Mat. et Tech.,* **33.**
Philippe, M. J., Wagner, F, and Esling, C. (1987). Proc. of Icotom 8, Santa Fe, to be published.
Philippe, M. J., Wagner, F., Esling, C. and Charquet, D. (1988). submitted to Zirconium in Nuclear Industry, San Diego.
Price, P. B. (1960). *Phil. Mag,* **5,** 873.
Reed-Hill, R. W. (1963). *Deformation Twinning,* Gordon and Breach 295.
Reed-Hill, R. E. (1971). *The Inhomogeneity of Plastic Deformation,* ASM, 285.
Reed-Hill, R. E. (1972). *Reviews of high temperatures materials,* **1,** 99.
Reed-Hill, R. E., Donoso, F. R. and Garde, A. M. (1975). *Met. Trans.* **6,** 1292.
Rosi, F. D., Dube, C. A. and Alexander, B. H. (1953). *J. of Metals,* 257.
Rosi, F. D., Perkins, F. C. and Seigle, S. S. (1956). *Trans. Met. Soc. AIME,* **206,** 115.
Sztwiertnia, K., Mueller, H. and Haessner, F. (1985). *Mat. Scien. and Tech.,* **1,** 380.
Taylor, G. I. (1938). *J. Inst. Metals* **62,** 307.
Tenckhoff, E. (1978). *Met. Trans.,* **9A,** 1401.
Tenckhoff, E. *Verformungsmechanismen, Textur und Anisotropie in Zirkonium und Zircaloy,* Gebruder Borntraeger, Berlin Stuttgart 1980.
Thornburg, D. R. (1971). Thesis Carnegie Mellon University, Pittsburgh, Pennsylvania, USA.
Thornburg, D. R. and Piehler, H. R. (1973). *Titanium Science and Technology, Vol.* **2,** Plenum Press, 1187.
Thornburg, D. R. and Piehler, H. R. (1975). *Met. Trans.,* **6A,** 1511.
Tome, C. and Kocks, U. F. (1984). *Acta Met.*
a) Van Houtte, P. and Aernoult (1975). *Z. Metallkde,* **66,** 202.
b) Van Houtte, P. (1975). Thesis Dept. Metaalkunde, Katholike Universited Leuven.
Vöhringer, (1969). *Mat. Sci. and Eng,* **3,** 299, 1968.
Wassermann, G. and Grewen, J. (1962). *Texturen metallischer Werkstoffe* Springer Verlag.
Williams, D. N. and Eppelsheimer, D. S. (1952). *Nature,* **170,** 146.
Williams, D. N. and Eppelsheimer, D. S. *J of Metals,* 1378.
Wonsiewich, B. C., and Backofen, W. A. (1967). *Trans. Met. Soc. AIME,* **239,** 1422.
Yoo, M. H. (1981). *Metal. Trans.* **12A,** 409.